Identification of the dinitrogen ⟨001⟩ split interstitial H1a in diamond

S. Liggins,[1] M. E. Newton,[1] J. P. Goss,[2] P. R. Briddon,[2] and D. Fisher[3]
[1]*Department of Physics, University of Warwick, Coventry CV4 7AL, United Kingdom*
[2]*EECE, Newcastle University, Newcastle Upon Tyne NE1 7RU, United Kingdom*
[3]*Diamond Trading Company (DTC) Research Centre, Belmont Road, Maidenhead, Berkshire SL6 6JW, United Kingdom*
(Received 16 October 2009; published 23 February 2010)

The structure of the defect responsible for the H1a absorption feature in diamond has been much debated. In this work, the results of uniaxial stress-splitting studies are compared to piezospectroscopic stress-splitting parameters calculated for the ⟨001⟩ dinitrogen split interstitial (N_{2I}) defect. The stress-splitting data shows that the H1a absorption band arises from an $A \rightarrow E$ transition at a center with D_{2d} symmetry. Furthermore, the experimentally and theoretically determined stress-splitting parameters are in excellent agreement, supporting the assignment of the H1a band to the N_{2I} defect.

DOI: 10.1103/PhysRevB.81.085214 PACS number(s): 81.05.U−, 61.72.jj, 52.70.Kz, 61.72.Bb

I. INTRODUCTION

Diamond is a material which possesses a combination of exceptional intrinsic properties useful for a wide range of technological and industrial applications.[1] Many of these properties are limited or even controlled by lattice defects and impurities grown into the material or introduced by post-growth processing. The effects of high-pressure high-temperature (HPHT) treatment, irradiation damage, and ion implantation are becoming better understood and controlled. However, there are still unresolved problems related to the formation and interaction of relatively simple point defects.

The process of irradiation with particles of sufficient energy displaces carbon atoms from their lattice position, creating defects such as self-interstitials and vacancies in the diamond lattice.[2] Isolated vacancies in both the negative (V^-) and neutral (V^0) charge states have been well characterized by both optical[3–8] and electron-paramagnetic-resonance (EPR) spectroscopy.[9,10] Self-interstitials have also been extensively studied with much consideration being given to potential recombination processes and new defects that may arise upon annealing.[11–15]

A common impurity in both natural and synthetic diamond is nitrogen and this forms the basis for the classification of the material.[16] Those diamonds that contain nitrogen in sufficient quantities to be detectable by infrared absorption are labeled type I and further subdivided into type Ia, in which nitrogen is present in aggregated forms, and type Ib, where nitrogen is predominantly in single substitutional form (N_S). Common structures of aggregated nitrogen are: nearest-neighbor substitutional nitrogen pairs, termed the *A* center; four substitutional nitrogen atoms surrounding a vacant lattice site (vacancy), labeled the *B* center; and three substitutional nitrogen atoms neighboring a vacancy, labeled N3.[16]

The interaction of irradiation-produced vacancies with nitrogen in diamond has been the subject of much study. A great deal is known and reported about both the neutral and negatively charged nitrogen-vacancy centers ($NV^{0/-}$),[17–20] the formation of which is dependent on the initial concentration of neutral single substitutional nitrogen (N_S^0) in the diamond.[6] Where nitrogen is present in significant concentrations, charge transfer[21] from the N_S^0 donor leads to the creation of V^- and N_S^+. When annealed to temperatures greater than 600 °C, N_S can trap vacancies to create nitrogen-vacancy complexes,[8]

$$N_S^0 + V \rightleftharpoons N_S^+ + V^-,$$

$$N_S^0 + V \rightarrow NV^0,$$

$$NV^0 + N_S^0 \rightarrow NV^- + N_S^+. \quad (1)$$

At higher temperatures vacancy-enhanced aggregation may occur, leading to the recycling of the vacancy in multiple reactions,[22]

$$NV + N \rightharpoonup N_S - N_S + V,$$

$$N_S + V \rightarrow NV. \quad (2)$$

The understanding of the interactions of self-interstitials and nitrogen is far less developed. It is known that the di-interstitial, labeled R1,[13] is not produced in diamonds where the concentration of nitrogen present in the lattice is far greater than the concentration of interstitials produced as a result of irradiation.[23] However, the production of the isolated interstitial (I_{001}) is unaffected by the concentration of N_S,[14] showing the preference for the neutral charge state of the interstitial despite the presence of a deep donor.[23]

In recent work, two new spin one-half defects have been identified by EPR, which has shown their properties to be consistent with them being the ⟨001⟩-nitrogen split interstitial (N_I) as illustrated in Fig. 1(a) and the ⟨001⟩-nitrogen split interstitial-⟨001⟩-carbon split interstitial pair (N_I-I_{001}).[24] This rebuts the proposal by Kiflawi *et al.* [Fig. 1(b)] that the nitrogen interstitial adopts a bond-centered interstitial structure, which was proposed as a potential model for the H1a absorption band.

It has been demonstrated that the incorporation of nitrogen in HPHT-grown diamond is sector dependent, with ⟨111⟩ sectors showing the highest N_S concentrations and ⟨110⟩ sectors substantially less.[25] Both the N_I and N_I-I_{001} defects were observed in lightly nitrogen-doped sectors and it was suggested that they were electron traps, such that in heavily

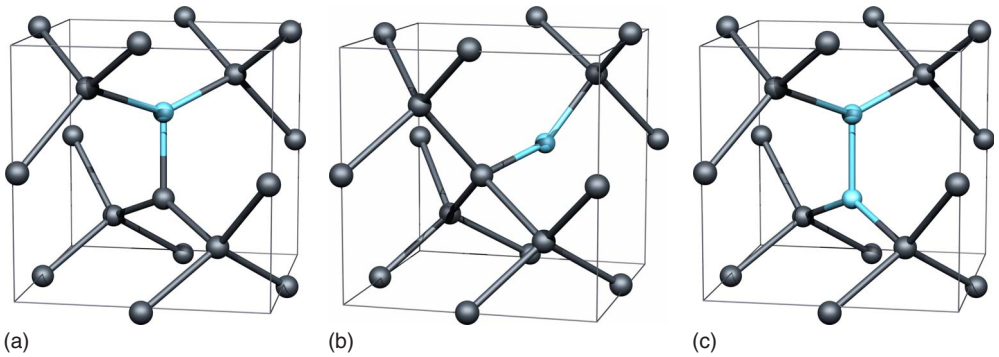

FIG. 1. (Color online) Various potential interstitial-related structures involving nitrogen atom in diamond. The cube of side length a_0 indicates the lattice cubic direction. (a) and (b) show the ⟨001⟩-oriented split interstitial (Ref. 27) and puckered bond-centered (Ref. 29) models for N_I, respectively. (c) shows the dinitrogen ⟨001⟩ split interstitial center model for H1a (Ref. 27). In all structures the light (blue) and dark (gray) atoms are N and C, respectively.

doped material where $[N_S] \gg [V], [I]$, the defects would be in a negatively charged state and hence not detectable by EPR.

Theory and experiment of these defects' existence and observation appear to be broadly in accord.[24] The activation energy[26] for migration of the I_{001} is 1.6 eV but radiation-enhanced interstitial migration has been reported.[12] Once mobile, it is postulated that I_{001} interstitials are trapped by N_S^0 producing N_I^0,

$$I_{001} + N_S^0 \rightarrow N_I^0,$$

$$N_I^0 + N_S^0 \rightleftharpoons N_I^- + N_S^+. \tag{3}$$

It is unlikely that N_I^0 would revert back to I_{001} and N_S^0 but migrate as itself once mobile. Goss *et al.* predicted that the barrier to migration for N_I^- is substantially less than that for N_I^0.[27] The capture of I_{001} by N_I would produce N_I-I_{001}, an R1-like defect, with one of the threefold-coordinated carbons replaced by a nitrogen atom,

$$I_{001} + N_I^0 \rightarrow (N_I\text{-}I_{001})^0. \tag{4}$$

In high nitrogen regions, charge transfer could occur,

$$(N_I\text{-}I_{001})^0 + N_S^0 \rightleftharpoons (N_I\text{-}I_{001})^- + N_S^+. \tag{5}$$

Capture of N_I by N_S would produce N_{2I} which is the defect proposed to be responsible for the infrared H1a absorption band [Fig. 1(c)].[27] Here, both dumbbell atoms of the interstitial are replaced by nitrogen atoms,

$$N_I + N_S \rightarrow N_{2I}. \tag{6}$$

We speculate that the barrier to formation of Eq. (6) could be reduced if the reactants were in the negative and positive charge states, permitting the migration of the nitrogen interstitial and the formation of the H1a band at 650 °C in type Ib materials. For example,

$$N_I^- + N_S^+ \rightarrow N_{2I}. \tag{7}$$

This is in response to Felton *et al.* highlighting the stability of N_I^0 at 1400 °C.[24]

Goss *et al.* proposed that N_{2I} could be produced by capture of the I_{001} by an A center such that

$$I_{001} + N_S - N_S \rightarrow N_{2I} \tag{8}$$

which could occur at 300 °C where the formation of the H1a band is seen in type Ia diamond.

This could explain the different temperatures required to produce the H1a absorption band in type Ia diamond, since the mobility of I_{001} is required, whereas in type Ib diamond, it is the mobility of N_I^- that is the key factor.[27] For a review of the annealing behavior of the H1a absorption band and for details of the proposed models of the centers illustrated in Fig. 1, the reader is directed to the paper by Goss *et al.*[27]

The calculated thermal stability of N_{2I} supports the assignment of N_{2I} as the defect responsible for the H1a band. The superficial contradiction of the ^{14}N-^{15}N mixed-isotope data (not indicating a vibration from a mixed-isotope center and therefore suggesting the band to arise from the motion of a single nitrogen atom), is explained by a degenerate pair of vibrational modes (*E* mode), shown in Figs. 2(a) and 2(b), of the dinitrogen system, which shows the significant interaction between the nitrogen atoms with only one of the nitrogen atoms being involved in each mode.[27] Furthermore, the mode involves two equivalent carbon atoms, which is consistent with the ^{12}C:^{13}C isotope splitting of the H1a band.[28]

The assignment of the H1a mode to N_{2I} with a proposed structure as illustrated in Fig. 1(c), could essentially be confirmed by data showing that the absorption mode originates from a defect with D_{2d} symmetry and is an $A \rightarrow E$ transition, so long as the experimental piezospectroscopic parameters are consistent with those determined for the N_{2I} model. The predicted high symmetry of the defect and the degeneracy of the local-vibrational mode, suggests that a convincing assignment could be made using the splitting patterns and rates under uniaxial stress along high-symmetry crystallographic directions.

II. UNIAXIAL STRESS

The application of uniaxial stress is a well-established technique for identifying the symmetry of a defect and probing the nature of the transition. Strain is introduced into the system forcing the movement of atoms, which in turn alters the electron-nuclear interactions. Extensive tabulations have

TABLE I. Tabulated shift and splitting patterns for the D_{2d} center displaying and $A \rightarrow E$ transition according to the direction of applied stress.

Direction	Transition energy	$E_{\parallel}:E_{\perp}$
[001]	$\hbar\omega+A_1\sigma$	0:1
	$\hbar\omega+(A_2+B)\sigma$	0:1
	$\hbar\omega+(A_2-B)\sigma$	2:0
[111]	$\hbar\omega+\frac{1}{3}(A_1+2A_2+C)\sigma$	4:1
	$\hbar\omega+\frac{1}{3}(A_1+2A_2-C)\sigma$	0:3
		$E_{110}:E_{001}:E_{1\bar{1}0}$
[110]	$\hbar\omega+\frac{1}{2}(A_1+A_2+B)\sigma$	0:2:0
	$\hbar\omega+\frac{1}{2}(A_1+A_2-B)\sigma$	1:0:1
	$\hbar\omega+(A_2+\frac{1}{2}C)\sigma$	1:0:0
	$\hbar\omega+(A_2-\frac{1}{2}C)\sigma$	0:0:1

been prepared and published for the effects of stress on centers of different symmetry in cubic crystals.[30–33] The application of uniaxial stress has the effect of perturbing the electronic and vibrational states of a center and lifting its degeneracy.

In cubic crystals, the stress tensor, $\boldsymbol{\sigma}$, is defined as

$$\boldsymbol{\sigma_{ij}} = \sigma\cos(\theta_i)\cos(\theta_j) = \begin{pmatrix} \sigma_{xx} & \sigma_{xy} & \sigma_{xz} \\ \sigma_{yx} & \sigma_{yy} & \sigma_{yz} \\ \sigma_{zx} & \sigma_{zy} & \sigma_{zz} \end{pmatrix},$$

where σ is the magnitude of the stress and θ_i and θ_j the angles between the applied stress and the ith and jth cubic axis. $\boldsymbol{\sigma}$ is symmetric and therefore stresses where $i=j$ represent compression stresses whereas $i \neq j$ characterizes shear stresses. In application, when directed along ⟨001⟩, symmetric σ_{ii} stress is generated and when along ⟨111⟩, shear σ_{ij} stress is induced. Stressing along the ⟨110⟩ direction applies both forms and therefore can act as a consistency check.

The shift and splitting of states can be expressed by a set of independent parameters. The theory behind the calculation of these parameters is well expressed in papers by Kaplyanskii and Hughes.[30,34] The result is the ability to tabulate the energy shifts of lines in the uniaxial stress spectra.

Important to this paper are those for the tetragonal D_{2d} center (Table I). These tables indicate expected transition energies and the ratio of peak intensities to occur at these energies under different polarizations. Solutions for the parameters can therefore be calculated by assigning the theoretical transition energies to the experimental peaks and solving simultaneously to optimize the fit.

III. EXPERIMENTAL DETAIL

Two HPHT grown samples, each enriched with 95% ^{15}N (~150 ppm as grown), were polished such that sample A had faces suitable for stress along the ⟨001⟩ and ⟨110⟩ directions and sample B was prepared for stress in the ⟨111⟩ direction. The accuracy of the face plane orientation was to within $\pm 1°$, confirmed by Laue back reflection of x-ray diffraction. Samples were polished such that they were free from, under ×10 magnification, inclusions, cracks and chips which could act as fracture propagation sites. Both samples were of the approximate size $1\times1\times2$ mm. Irradiation was performed using 1.5 MeV electrons to a dose of 1.5×10^{18} e^-/cm^2 for sample A and 1.0×10^{18} e^-/cm^2 for sample B, followed by annealing in an oxygen free, nitrogen-rich environment at a temperature of 1000 °C.

For the investigation of annealing behavior, a type Ib sample was annealed at 200 °C intervals from 800 to 1400 °C and 100 °C thereafter for 4 h in an oxygen free, nitrogen-rich environment. Characterization of the intensity of the H1a absorption band was then made using infrared spectroscopy.

Isotopic shift studies were made using one of the ^{15}N stress samples (sample B) and a sample grown with a natural abundance of nitrogen which was also annealed to 1000 °C post irradiation at 1.0×10^{18} e^-/cm^2.

Stress investigations were performed using a custom-built stress cell in conjunction with a PerkinElmer Spectrum GX Fourier-transform infrared spectrometer equipped with a beam condenser. All measurements were taken at room temperature using a resolution of 1 cm^{-1}. Spectra were taken for stress applied along the three principal directions with the electric field vector polarized both parallel and perpendicular to the direction of stress using an Edmund optics zinc selenide holographic wire grid polarizer.

IV. THEORETICAL DETAIL

Candidate structures for the H1a center were modeled using density-functional calculations within the local-density approximation[35] as implemented in the AIMPRO (*ab initio* modeling program) code.[36,37] The wave-function basis consists of atom-centered Gaussians.[38] Carbon is treated using fixed linear combinations of s and p orbitals with the addition of a set of d functions to allow for polarization, with a total of 13 functions per atom. Nitrogen is treated using independent sets of s, p, and d Gaussians with four widths, yielding 40 functions per atom. The charge density is Fourier transformed using plane waves with a cutoff of 350 Ry, yielding well-converged total energies. Core electrons are eliminated by using norm-conserving pseudopotentials.[39] The lattice constant and bulk modulus of bulk diamond are, respectively, reproduced to within ~1% (an overestimate) and 2% (underestimate) of experiment. The calculated direct and indirect band gaps agree with published plane-wave values.[40]

The defects are represented using periodic boundary conditions, with cells containing 64 host sites in a simple cubic arrangement and periodic wavelength of $2a_0$. The Brillouin zone was sampled using the Monkhorst-Pack scheme with a uniform mesh of $2\times2\times2$ special k points.[41] Calculation of the variation in energy with lattice constant for a denser sample of $4\times4\times4$ indicates very small quantitative differences (<0.2 meV/atom) from the coarser scheme and a equilibrium lattice constant within 10^{-3} Å. We judge the $2\times2\times2$ sampling to be sufficiently converged.

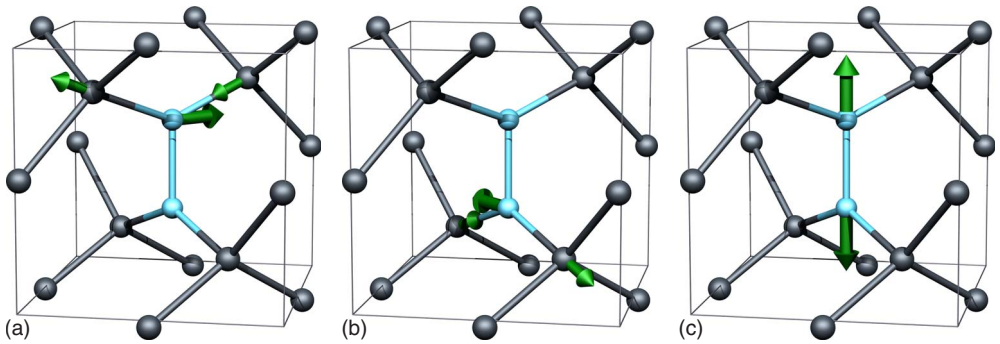

FIG. 2. (Color online) Proposed normal modes of the dinitrogen split interstitial. (a) and (b) show the two components of the E mode assigned to H1a, and (c) the A_1, IR-inactive mode discussed in the text. The central two, light (blue) atoms are nitrogen and the cube of side length a_0 indicates the lattice cubic direction. The arrow shows the displacements during the modes of vibration, their lengths indicating relative amplitude on different atom sites.

Deformation of the supercell under strain assumed an isotropic, homogeneous elastic medium, characterized by Young's modulus, E, for which we take the value[42] of 1223 GPa and the Poisson ratio, ν, for which a calculated value[43] of 0.1 was used. For varying strains, force constants were obtained by displacing atoms in each of the x, y, and z directions by 0.026 Å and evaluating the forces on each atom in the cell. Hence, second derivatives of the energy with respect to displacement is obtained using a finite difference formula using the analytic forces and the quasiharmonic dynamical matrix built in the usual way. Diagonalization yielded vibrational frequencies as a function of strain, or as a function of stress using the Young's modulus.

V. RESULTS

Due to the use of ^{15}N-enriched samples, the 1450.8(2) cm^{-1} feature labeled H1a was shifted to 1426.7(2) cm^{-1} as shown in Fig. 3. This is in agreement with the reported shift expected for this isotopic substitution.[29] As Fig. 3 indicates, the ^{15}N sample still contained a small fraction of ^{14}N. This is highlighted by the detectable absorption feature at 1450.8(2) cm^{-1} in the related spectrum.

The annealing behavior of H1a, shown in Fig. 4, is broadly consistent with previously published results. While it is generally reported that the H1a absorption feature is seen to begin to anneal out at 1100 °C and have completely annealed out by 1400 °C, these experiments report that values of 1200 and 1600 °C would be more appropriate. Maximum intensity of the H1a absorption feature has subsequently been assessed to be near maximum and easily achievable without risk of graphitization or sample damage, at a temperature of 1000 °C and it was at this temperature that the irradiated samples were annealed to create the H1a absorption feature for the uniaxial stress experiments.

Assessment of the total concentration of nitrogen in the sample (N_S^0 by EPR and IR, N_S^+ by IR, NV^- by optical absorption and NV^0 by EPR) post various stages in annealing, showed a rising deficit as the intensity of H1a increased. This would be expected since H1a is known to involve nitrogen from the isotopic substitution experiment results. It is unlikely that H1a is the only source of the nitrogen deficit since other nitrogen-related complexes, beyond those mentioned, are known to form.

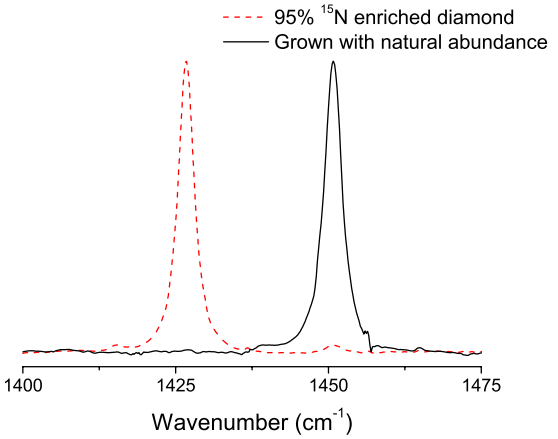

FIG. 3. (Color online) Spectra highlighting the isotopic shift of the H1a absorption band in ~95% ^{15}N-enriched diamond compared to a sample grown with a natural abundance of nitrogen (^{14}N:^{15}N, 99.63:0.37). Intensities here have been scaled to give the same peak height for both spectrums.

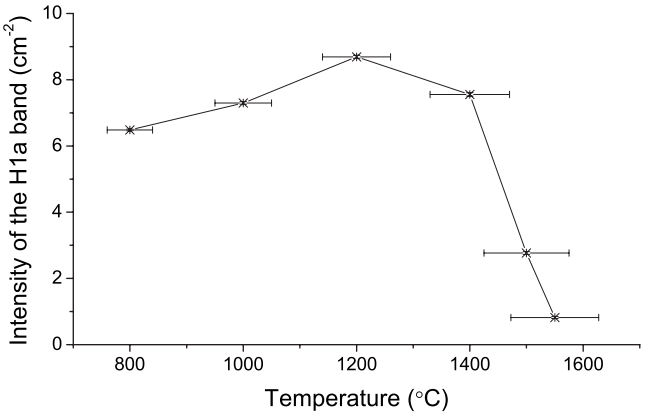

FIG. 4. Isochronal annealing study of H1a in a ^{15}N sample. Samples were annealed at increasing temperatures for 4 h. H1a is seen to be stable to 1200 °C beyond which it is seen to decrease in intensity and anneal out by 1600 °C.

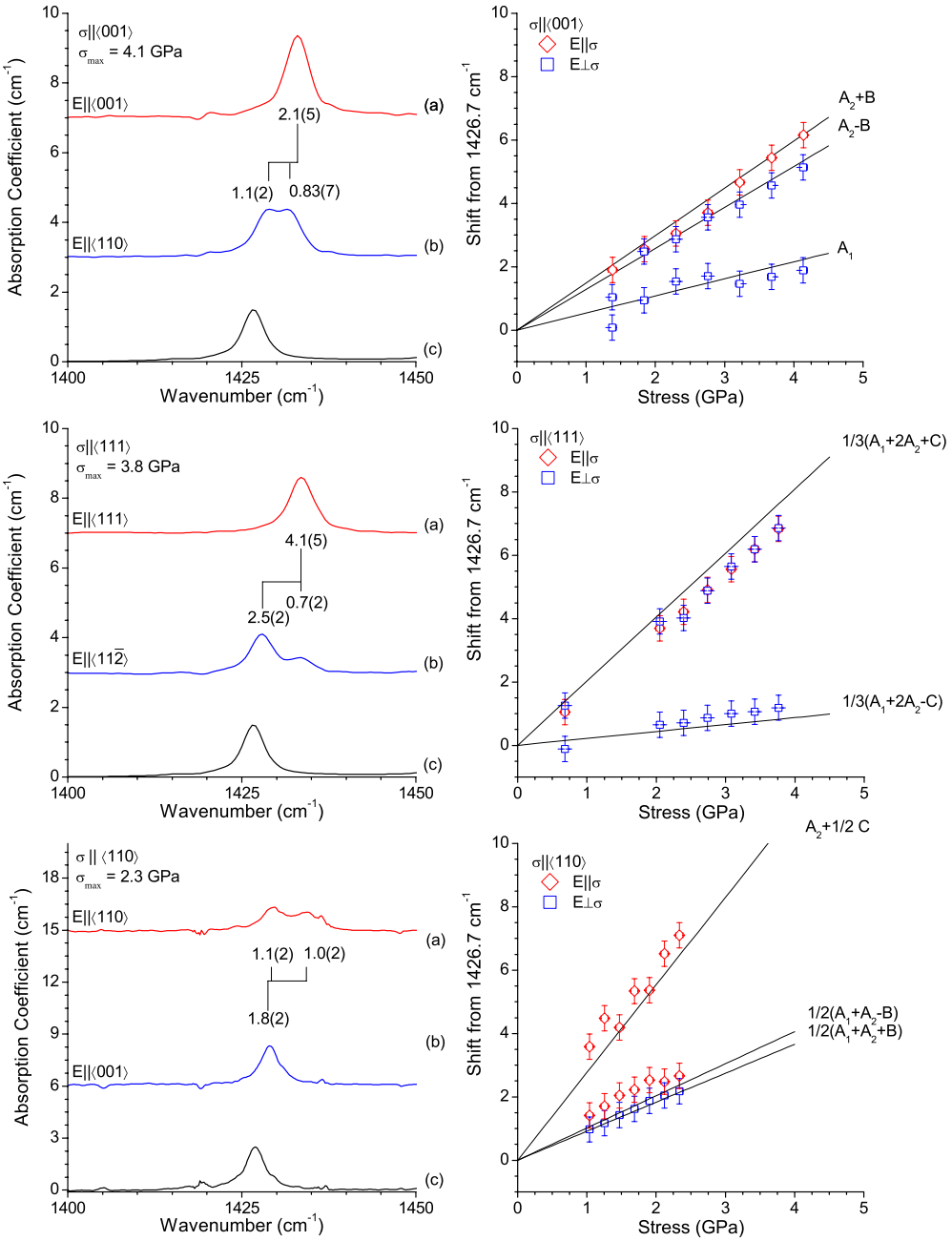

FIG. 5. (Color online) The left column illustrates spectra attained at 4.1, 3.8, and 2.3 GPa for $\sigma\|\langle 001\rangle$, $\langle 111\rangle$, and $\langle 110\rangle$ directions, respectively, which have been offset for clarity. Spectra (a) and (b) in each, represent the sample under stress and spectrum (c), the sample under zero stress. The right column shows the transition frequencies as a function of stress compared to the best fit parameters from all the data for an $A \rightarrow E$ transition at a D_{2d} center.

Figure 5 shows the experimental stress splitting data with the applied stress along ⟨001⟩, ⟨111⟩, and ⟨110⟩ directions. The solid lines show the best fit to an $A \rightarrow E$ transition at a defect with D_{2d} symmetry (Table I) using the piezospectroscopic parameters,

$$
\begin{aligned}
{}^{\mathrm{exp}}A_1 &= +0.54(9)\ \mathrm{cm}^{-1}\ \mathrm{GPa}^{-1},\\
{}^{\mathrm{exp}}A_2 &= +1.39(5)\ \mathrm{cm}^{-1}\ \mathrm{GPa}^{-1},\\
{}^{\mathrm{exp}}B &= -0.10(9)\ \mathrm{cm}^{-1}\ \mathrm{GPa}^{-1},\\
{}^{\mathrm{exp}}C &= +2.75(9)\ \mathrm{cm}^{-1}\ \mathrm{GPa}^{-1}. \qquad (9)
\end{aligned}
$$

It should also be noted that the relative intensities of the components of the stress split H1a band are in good accord with theory (Table I).

The most substantial parameters ($^{\mathrm{exp}}A_2$ and $^{\mathrm{exp}}C$) represent the response to pseudohydrostatic and shear forces on the system.

VI. THEORETICAL MODELING: THE DINITROGEN MODEL FOR H1a

As outlined above, the proposed model for the H1a vibrational center is pair of N atoms replacing a single host atom [Fig. 1(c)]. The calculated vibrational properties of this D_{2d} center includes one mode at 1442 cm^{-1} in ^{14}N diamond and 1418 cm^{-1} in ^{15}N diamond (close to the observed lines at

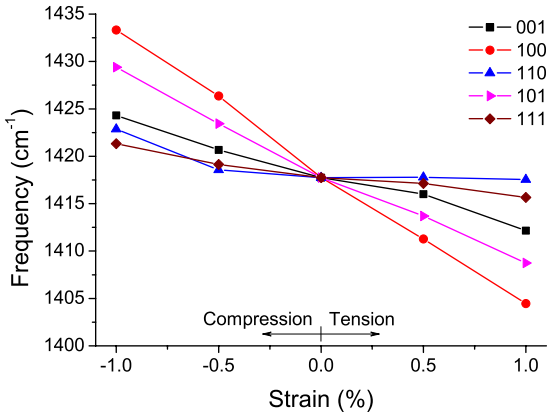

FIG. 6. (Color online) Calculated frequencies as a function of strain along high-symmetry directions for the interstitial ^{15}N-pair model with the (N-N bond aligned along [001]) for the H1a model.

1450.8(2) cm^{-1} and 1426.7(2) cm^{-1} respectively), which is twofold degenerate (an E mode). This mode of vibration, indicated in Fig. 2(a), also helps explain the results seen in nitrogen isotopic investigations which might otherwise rule out a dinitrogen model. The strain response for this particular model is plotted in Fig. 6 and the calculated shift rates are listed in Table II.

The twofold degeneracy under zero strain is raised for all strain directions except along [001] for centers oriented parallel to the strain. Additional splittings occur for differently orientated centers (Fig. 6). For example, strain in the [001] direction yields an E mode for centers aligned along [001] [Figs. 2(a) and 2(b)] but for [100] and [010] aligned centers the E mode is split, albeit to a modest extent.

Values for the piezospectroscopic parameters ($^{\text{th}}A_1$, $^{\text{th}}A_2$, $^{\text{th}}B$, $^{\text{th}}C$) can be determined from the calculated strain response for the E mode of N_{2I}. The theoretical values are given below,

$$^{\text{th}}A_1 = +0.50 \text{ cm}^{-1} \text{ GPa}^{-1},$$

$$^{\text{th}}A_2 = +1.45 \text{ cm}^{-1} \text{ GPa}^{-1},$$

$$^{\text{th}}B = -0.15 \text{ cm}^{-1} \text{ GPa}^{-1},$$

$$^{\text{th}}C = +2.10 \text{ cm}^{-1} \text{ GPa}^{-1}. \quad (10)$$

Returning to the dinitrogen interstitial defect, in addition to the E mode assigned to the H1a band, we note that there are other modes of vibration associated with this structure. Of these, the only other mode that is calculated to lie above the diamond one-phonon maximum is an A_1 mode related to the bond stretch along the N-N axis [Fig. 2(c)]. This is IR inactive, i.e., the vibrational mode is not associated with changes in the induced electric dipole. In contrast to the mode assigned to H1a, this A_1 mode does exhibit mixed-isotope splittings characteristic of two N atoms (1830 cm^{-1}:1800 cm^{-1}:1768 cm^{-1} $\equiv$ ^{14}N-^{14}N:^{14}N-^{15}N:^{15}N-^{15}N).[27] In principle, this could be detected in a Raman-scattering experiment, provided a sufficient concentration of defect centers could be introduced. Predictions of the strain responses for this nondegenerate mode are also listed in Table II.

The possibility exists that there are other modes that might be present in the IR spectra. For example, that where the two nitrogen atoms are vibrating in unison along their bond direction (a B_2, IR-active mode), is calculated to occur at a frequency less than 1332 cm^{-1}, and it is probable that this mode is present but resonant with the diamond one-phonon band.

TABLE II. Calculated linear shift rates for the E modes and A_1 local-vibrational modes of the dinitrogen interstitial pair model for H1a for ^{14}N and ^{15}N pairs. All values are presented in units of cm^{-1} per percent strain for a [001]-oriented dinitrogen center, and are obtained using a least-squares fit to the calculated data. The errors in the fits are estimated to be less than 1 cm^{-1} per percent strain.

	Shift rates			
	E		A_1	
Direction	^{14}N	^{15}N	^{14}N	^{15}N
[001]	−6	−6	−15	−14
[100]	−15	−15	−9	−10
	−18	−18		
[110]	−2	−2	−7	−7
	−33	−31		
[101]	−10	−10	−14	−13
	−12	−12		
[111]	−3	−3	−10	−10
	−23	−22		

VII. CONCLUSIONS

A combination of experimental uniaxial stress studies and atomistic modeling has been used to investigate the symmetry and vibrational modes of the defect responsible for the H1a band observed in irradiated and annealed nitrogen-doped diamond.

The uniaxial stress splitting data of the H1a band shows beyond doubt that this feature originated from a doubly degenerate local-vibrational mode for a defect with D_{2d} symmetry. The energy of the E mode calculated for the N_{2I} defect is in very good agreement with the experimental data for the H1a absorption band for all combinations of nitrogen isotopes. The agreement between the experimentally determined piezospectroscopic parameters of H1a and those calculated for the E mode of N_{2I}, are outstanding. This leads to the conclusion that the ⟨001⟩ dinitrogen split interstitial N_{2I} is the only plausible model for the defect responsible for the H1a mode.

The theoretical modeling also predicts an infrared inactive but Raman-active A_1 N_I-N_I stretch mode for N_{2I}. This A_1

mode is predicted to exhibit mixed-isotope splitting and resolvable splitting under uniaxial stress.[27]

This result encourages the calculation of piezospectroscopic parameters for the vibrational modes of other defects in diamond. Such an approach would be very useful for assigning vibrational modes, which originate from defects of the same symmetry but which have substantially different piezospectroscopic parameters, to the correct atomistic model.

ACKNOWLEDGMENTS

The authors would like to thank Joh Hansen (formerly of Element Six, South Africa) and Jim Butler (of the Naval Research Laboratory, USA) for their efforts with sample growth and preparation. Additionally, the DTC Research Center and Science City are thanked for their financial support of this project.

[1] C. J. Wort and R. S. Balmer, Mater. Today **11**, 22 (2008).
[2] B. Campbell, W. Choudhury, A. Mainwood, M. Newton, and G. Davies, Nucl. Instrum. Methods Phys. Res. A **476**, 680 (2002).
[3] G. Davies and E. C. Lightowlers, J. Phys. C **3**, 638 (1970).
[4] C. D. Clark and J. Walker, Proc. R. Soc. London, Ser. A **334**, 241 (1973).
[5] G. Davies and C. M. Penchina, Proc. R. Soc. Lond., Ser. A **338**, 359 (1974).
[6] G. Davies, Nature (London) **269**, 498 (1977).
[7] G. Davies and C. Foy, J. Phys. C **13**, 2203 (1980).
[8] G. Davies, S. C. Lawson, A. T. Collins, A. Mainwood, and S. J. Sharp, Phys. Rev. B **46**, 13157 (1992).
[9] J. Isoya, H. Kanda, Y. Uchida, S. C. Lawson, S. Yamasaki, H. Itoh, and Y. Morita, Phys. Rev. B **45**, 1436 (1992).
[10] J. A. van Wyk, O. D. Tucker, M. E. Newton, J. M. Baker, G. S. Woods, and P. Spear, Phys. Rev. B **52**, 12657 (1995).
[11] D. C. Hunt, D. J. Twitchen, M. E. Newton, J. M. Baker, T. R. Anthony, W. F. Banholzer, and S. S. Vagarali, Phys. Rev. B **61**, 3863 (2000).
[12] M. E. Newton, B. A. Campbell, D. J. Twitchen, J. M. Baker, and T. R. Anthony, Diamond Relat. Mater. **11**, 618 (2002).
[13] D. J. Twitchen, M. E. Newton, J. M. Baker, O. D. Tucker, T. R. Anthony, and W. F. Banholzer, Phys. Rev. B **54**, 6988 (1996).
[14] D. C. Hunt, D. J. Twitchen, M. E. Newton, J. M. Baker, J. K. Kirui, J. A. van Wyk, T. R. Anthony, and W. F. Banholzer, Phys. Rev. B **62**, 6587 (2000).
[15] H. E. Smith, G. Davies, M. E. Newton, and H. Kanda, Phys. Rev. B **69**, 045203 (2004).
[16] I. Kiflawi and S. C. Lawson, in *Properties, Growth and Applications of Diamond*, emis Datareviews Series No. 26, edited by M. H. Nazaré and A. J. Neves (INSPEC, London, 2001), Chap. A5.2, pp. 130–133.
[17] G. Davies and M. E. R. Hamer, Proc. R. Soc. Lond., Ser. A **348**, 285 (1976).
[18] G. Davies, J. Phys. C **12**, 2551 (1979).
[19] S. Felton, A. M. Edmonds, M. E. Newton, P. M. Martineau, D. Fisher, and D. J. Twitchen, Phys. Rev. B **77**, 081201(R) (2008).
[20] S. Felton, A. M. Edmonds, M. E. Newton, P. M. Martineau, D. Fisher, D. J. Twitchen, and J. M. Baker, Phys. Rev. B **79**, 075203 (2009).
[21] S. C. Lawson, D. Fisher, D. C. Hunt, and M. E. Newton, J. Phys.: Condens. Matter **10**, 6171 (1998).
[22] A. T. Collins, J. Phys. C **13**, 2641 (1980).
[23] G. A. Watt, M. E. Newton, and J. M. Baker, Diamond Relat. Mater. **10**, 1681 (2001).
[24] S. Felton, B. L. Cann, A. M. Edmonds, S. Liggins, R. J. Cruddace, M. E. Newton, D. Fisher, and J. M. Baker, J. Phys.: Condens. Matter **21**, 364212 (2009).
[25] R. C. Burns, V. Cvetkovic, C. N. Dodge, D. J. F. Evans, M.-L. T. Rooney, P. M. Spear, and C. M. Welbourn, J. Cryst. Growth **104**, 257 (1990).
[26] L. Allers, A. T. Collins, and J. Hiscock, Diamond Relat. Mater. **7**, 228 (1998).
[27] J. P. Goss, P. R. Briddon, S. Papagiannidis, and R. Jones, Phys. Rev. B **70**, 235208 (2004).
[28] A. T. Collins, G. Davies, H. Kanda, and G. S. Woods, J. Phys. C **21**, 1363 (1988).
[29] I. Kiflawi, A. Mainwood, H. Kanda, and D. Fisher, Phys. Rev. B **54**, 16719 (1996).
[30] A. Kaplyanskii, Opt. Spectrosc. **16**, 329 (1964).
[31] A. E. Hughes and W. A. Runciman, Proc. Phys. Soc. London **90**, 827 (1967).
[32] G. Davies and M. H. Nazare, J. Phys. C **13**, 4127 (1980).
[33] K. Mohammed, G. Davies, and A. T. Collins, J. Phys. C **15**, 2779 (1982).
[34] A. E. Hughes, Proc. Phys. Soc. London **87**, 535 (1966).
[35] J. P. Perdew and Y. Wang, Phys. Rev. B **45**, 13244 (1992).
[36] P. Briddon and R. Jones, Phys. Status Solidi B **217**, 131 (2000).
[37] M. Rayson and P. Briddon, Comput. Phys. Commun. **178**, 128 (2008).
[38] J. P. Goss, M. J. Shaw, and P. R. Briddon, in *Theory of Defects in Semiconductors*, Topics in Applied Physics Vol. 104, edited by D. A. Drabold and S. K. Estreicher (Springer, Berlin/Heidelberg, 2007), pp. 69–94.
[39] C. Hartwigsen, S. Goedecker, and J. Hutter, Phys. Rev. B **58**, 3641 (1998).
[40] D. A. Liberman, Phys. Rev. B **62**, 6851 (2000).
[41] H. J. Monkhorst and J. D. Pack, Phys. Rev. B **13**, 5188 (1976).
[42] S.-F. Wang, Y.-F. Hsu, J.-C. Pu, J. C. Sung, and L. G. Hwa, Mater. Chem. Phys. **85**, 432 (2004).
[43] R. Jones, J. P. Goss, and P. R. Briddon, Phys. Rev. B **80**, 033205 (2009).